J. Fluid Mech. (1984), *vol.* 146, *pp.* 181–201
Printed in Great Britain

Theoretical study of the transonic flow past wedge profiles with detached shock waves

By MICHEL ABBOUD
Institut für Strömungslehre und Strömungsmaschinen, Universität (TH) Karlsruhe

(Received 6 September 1983)

This report presents a numerical study of the two-dimensional, steady and inviscid flow of a perfect gas past wedge profiles with detached shock waves for free-stream Mach numbers between 1.05 and 1.44.

Utilizing the hodograph transformation, a boundary-value problem for the mixed flow is formulated in the hodograph plane and subsequently solved by a finite-difference scheme, iterating respectively between the elliptic and hyperbolic regions. The use of boundary-fitted coordinates and a graded lattice failed to achieve satisfactory results, owing to either convergence difficulties or numerical inaccuracies introduced through the coordinate generator. On the other hand, Cartesian coordinates presented no convergence problems and yielded accurate results.

After transforming the solution back to the physical plane, the flow field between the shock wave and the limiting Mach wave is determined. A comparison of the results with experiments and other theories shows a good agreement both for the pressure distribution on the wedge and for the shock stand-off distance.

Also of special interest is a quantitative comparison of the results with the small-disturbance theory (solution of the Tricomi equation) and the limiting case of the free-stream Mach number 1.

Moreover, an example of the flow past round-nosed wedges, with and without an angle of attack, is treated using the inverse method.

1. Introduction

In a supersonic flow past a wedge, depending on a combination of the free-stream Mach number and the wedge angle, three essentially different types of flow are possible, which have been discussed by Guderley (1947):

(i) attached bow wave with purely supersonic flow;
(ii) attached bow wave with mixed subsonic–supersonic flow;
(iii) detached bow wave with mixed subsonic–supersonic flow.

This paper is concerned with case (iii) of a mixed subsonic–supersonic flow with a detached bow wave, as shown qualitatively in figure 1.

In the following it is sufficient to restrict the discussion to the upper half of the plane. The procedure for the lower half is then obvious. The flow past the wedge (angle 2α, thickness $2h$) with free-stream Mach number $M_\infty > 1$ is from left to right. A detached shock wave is formed in front of the wedge, which decelerates the medium from a supersonic to a subsonic velocity and deflects the streamlines. As already indicated, a local subsonic field exists behind the bow wave in which the medium is accelerated to the sonic velocity on the sonic line BD and finally to a supersonic state. The sonic line leaves the ridge of the wedge in the point B and extends to the point D on the shock wave.

Behind the sonic line at the ridge B, a supersonic fan originates, which tends, in

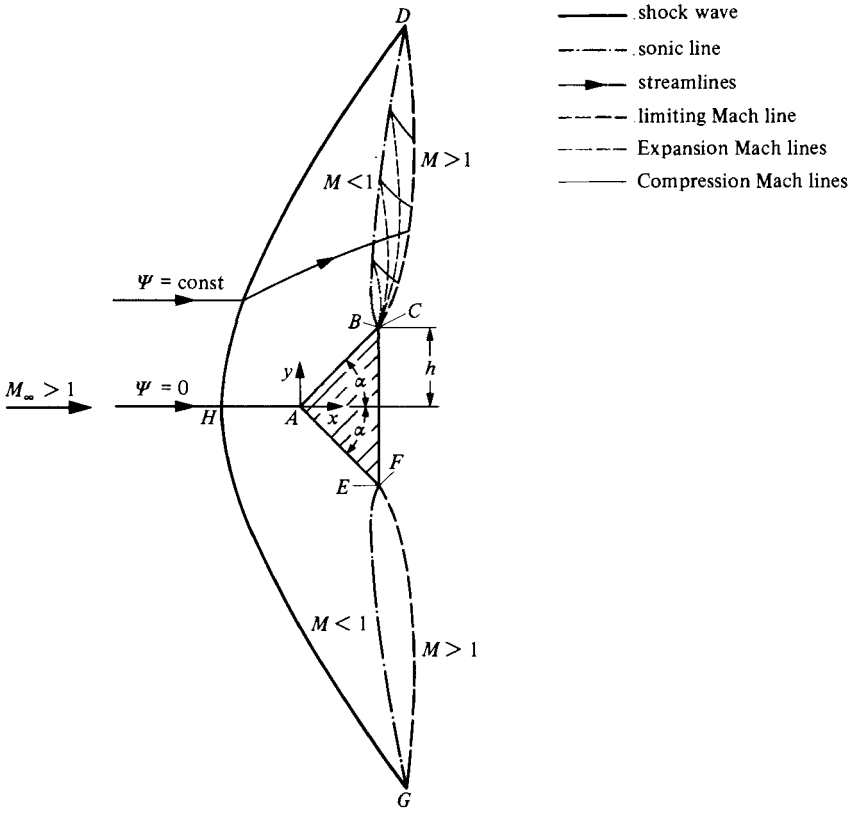

FIGURE 1. Flow field about a wedge with a detached shock wave.

the immediate vicinity of the ridge, toward a simple Prandtl–Meyer flow. Of special importance is the last expansion wave, which intersects the sonic line in the point D on the bow wave. This limiting Mach wave confines that part of the supersonic field which is able to influence the subsonic field. Thus a small disturbance downstream of the limiting wave BCD has no influence on the subsonic field. Hence the flow field downstream of the limiting Mach wave is a purely supersonic problem, whereas the field between the shock wave and the limiting wave is an interdependent subsonic–supersonic problem and must therefore be treated as a single bounded transonic zone.

Computations pertaining to this problem can be performed either in the physical or in the hodograph plane. Since this paper deals with the latter method, a short review of the existing work directly related to this study will be given.

In his original paper, Frankl (1945) formulated the boundary-value problem for the flow past a wedge profile with a detached bow wave and proved its uniqueness. Later, and independently of Frankl, Guderley (1947) simplified the exact boundary-value problem to small disturbances around the sonic velocity. Within the scope of this simplification, Guderley & Yoshihara (1950) solved analytically the modified boundary-value problem for the limiting case of a free-stream Mach number 1. Efforts by Vincenti & Wagoner (1952) to obtain a numerical solution of the problem (for the small-disturbance theory) failed, because they could not achieve convergence between the elliptic and hyperbolic regions. Nevertheless, they succeeded in obtaining a numerical solution after eliminating the supersonic domain from explicit consideration. In a later (1954) paper, they extended their work to include flows with a small angle of attack.

Vincenti, Wagoner & Fisher (1956) solved the exact equations and succeeded for the first time in treating the mixed flow past an inclined flat plate at a free-stream Mach number 1 by an iterative scheme between the elliptic and hyperbolic regions. Using a similar procedure, van Raay (1973) extended the problem at the same Mach number ($M_\infty = 1$) for the flow past arbitrary wedges without an angle of attack. Later and intensive endeavours of the same author (1978 private communication) to solve the problem for $M_\infty \gtrsim 1$ failed owing to convergence difficulties encountered earlier and (as a consequence of the small-disturbance theory) circumvented by Vincenti & Wagoner (1952). More recently, while the present work was well under way, Graefe (1980) avoided an iterative treatment of the mixed flow and succeeded in solving the problem for the flow past arbitrary wedges at free-stream Mach numbers $M_\infty \geqslant 1.2$.

In spite of this progress, little or no data are available that allow a comparison of (i) computations of the exact hodograph equations with experiments, (ii) the results of the exact theory with the small-disturbance theory, and (iii) the flow fields for $M_\infty \gtrsim 1$ with the limiting case of $M_\infty = 1$. This paper is therefore a further development of the existing work on the hodograph method and provides the information just mentioned as lacking.

2. Basic equations

Assuming a steady two-dimensional flow and neglecting the effects of viscosity and thermal conductivity, the laws of conservation of mass, momentum and energy yield the following equation for the stream function Ψ (Sauer 1960):

$$\left(1-\frac{u^2}{c^2}\right)\Psi_{xx}-2\frac{uv}{c^2}\Psi_{xy}+\left(1-\frac{v^2}{c^2}\right)\Psi_{yy}=\rho\left(w^2\frac{\partial\rho}{\partial s}-\rho T\right)\frac{\mathrm{d}s}{\mathrm{d}\Psi}, \tag{2.1}$$

where u and v are the velocity components in the x- and y-directions, w is the magnitude of the velocity, c the speed of sound, ρ the density, T the temperature and s the entropy. The relationships between the stream function Ψ and the velocity components u and v are given by

$$u=\frac{1}{\rho}\Psi_y, \quad v=-\frac{1}{\rho}\Psi_x. \tag{2.2}$$

Owing to the curvature of the bow wave, an entropy gradient exists across the streamlines and the field behind the shock wave is of necessity rotational. This change of entropy normal to the streamlines, however, is small for transonic problems, and its neglection is justifiable, as can indeed be verified by the computed results for the highest free-stream Mach number $M_\infty = 1.44$. Setting

$$\frac{\mathrm{d}s}{\mathrm{d}\Psi}=0, \tag{2.3a}$$

which, according to Crocco's theorem, is equivalent to the condition of irrotationality

$$\frac{\partial u}{\partial y}-\frac{\partial v}{\partial x}=0, \tag{2.3b}$$

(2.1) is greatly simplified to

$$\left(1-\frac{u^2}{c^2}\right)\Psi_{xx}-2\frac{uv}{c^2}\Psi_{xy}+\left(1-\frac{v^2}{c^2}\right)\Psi_{yy}=0. \tag{2.4}$$

Equation (2.4) is a second-order quasi-linear partial differential equation of mixed

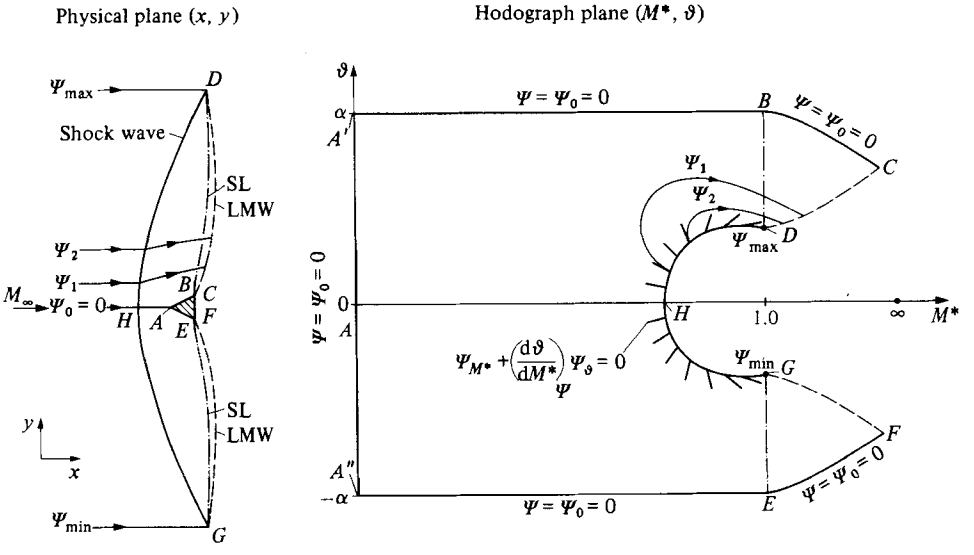

FIGURE 2. Mapping of the physical to the hodograph plane (SL ≡ sonic line, LMW ≡ limiting Mach wave).

type, where the boundary between the elliptic and the hyperbolic region is still unknown. Moreover, it represents a free boundary problem, because the extremities of the transonic zone that is to be investigated, namely the bow wave and the limiting Mach wave, are also unknown and must be determined as a part of the solution. These difficulties can be avoided, at the expense of numerical complications (as will be seen later), through the transformation of the problem to the hodograph plane.

3. Formulation of the problem in the hodograph plane

3.1. *Molenbroek–Chaplygin transformation*

The transition from the physical plane to the hodograph plane is accomplished through the Molenbroek–Chaplygin transformation (Ferrari & Tricomi 1968). The critical Mach number M^* and the direction ϑ of the velocity vector are employed as new independent variables instead of the physical coordinates x and y. Equation (2.4) then reduces to the Chaplygin equation:

$$M^{*2}\Psi_{M^*M^*} + M^* \frac{1-\frac{\kappa-3}{\kappa+1}M^{*2}}{1-\frac{\kappa-1}{\kappa+1}M^{*2}}\Psi_{M^*} + \frac{1-M^{*2}}{1-\frac{\kappa-1}{\kappa+1}M^{*2}}\Psi_{\vartheta\vartheta} = 0, \tag{3.1}$$

where κ is the ratio of the specific heats of the gas. Equation (3.1) is linear, and the boundary (i.e. sonic line) between the elliptic ($M^* < 1$) and hyperbolic regions ($M^* > 1$) is given by the relationship $M^* = 1$.

3.2. *Mapping the physical plane to the hodograph plane*

The mapping of the physical plane to the hodograph plane is shown in figure 2, and is limited for the present to the case of a zero angle of attack. The non-symmetrical case of an angle of attack will be discussed later.

The undisturbed oncoming flow characterized by the free-stream Mach number $M = M_\infty$ and $\vartheta = 0$ is mapped to the point ∞. The bow wave GHD appears as the subsonic portion of the shock polar. The stagnation streamlines $HABC$ and $HAEF$ run along the line of symmetry at $\vartheta = 0$, intersect the shock wave in the point H and proceed with a decreasing Mach number in the stagnation point A at the nose of the wedge. At A the streamline splits in two branches, which run along the upper and lower surface of the profile. The mapping of the stagnation streamline on the hodograph can then be described as follows. Before the shock wave the stagnation streamline is mapped again on the point ∞, jumps subsequently to the point of the normal shock H of the shock polar and proceeds at an angle $\vartheta = 0$ to the stagnation point A ($M = M^* = 0$), where ϑ takes all values between $+\alpha$ and $-\alpha$. The upper and lower surfaces of the wedge are given respectively by the horizontal lines $A'B$ at $\vartheta = \alpha$ and $A''E$ at $\vartheta = -\alpha$. The expansion fans at the wedge shoulders B and E appear respectively as the right-running wave BC and the left-running wave EF. Likewise the images of the limiting Mach lines are given through the left-running and right-running characteristics from the intersection of the shock wave GHD with the sonic lines BD and EG.

3.3. *Formulation of the boundary-value problem*

For a unique solution of the problem in the hodograph plane, the Chaplygin equation (3.1) has to be solved with the following boundary conditions (see e.g. Vincenti & Wagoner 1952):

$$\Psi = 0 \quad \text{on } FEA''A'BC, \tag{3.2a}$$

$$\Psi_{M^*} + \left(\frac{\mathrm{d}\vartheta}{\mathrm{d}M^*}\right)_\Psi \Psi_\vartheta = 0 \quad \text{on } GHD, \tag{3.2b}$$

$$\Psi = \Psi_{\max} \quad \text{in } D, \tag{3.2c}$$

$$\Psi = \Psi_{\min} \quad \text{in } G. \tag{3.2d}$$

In (3.2b) $(\mathrm{d}\vartheta/\mathrm{d}M^*)_\Psi$ is a lengthy expression for the slope of the streamlines on the shock polar, which can be determined from the deflection of the streamlines across the shock in the physical plane and which is given in detail by Abboud (1982). If the symmetrical case without an angle of attack is considered, the treatment can be restricted to the upper half of the plane ($\vartheta \geqslant 0$) with the additional boundary condition $\Psi = 0$ on AH. Graefe (1980) was the first to solve this boundary-value problem for $M_\infty \geqslant 1.2$ treating the whole domain as an elliptic one.

3.4. *Treatment of the problem at an angle of attack*

The treatment of the problem at an angle of attack is more involved, since the stagnation point moves from the nose (figure 3a) to the lower wedge surface, causing the development of a supersonic field with a shock wave at the leading edge (figure 3b). Depending on the wedge angle, a region of separation or cavitation may be expected. The representation of this complicated flow field in the hodograph is open to conjecture and would probably lie on several sheets. Guderley & Yoshihara (1953) and later Vincenti & Wagoner (1954) treated the flow past thin wedges at a very small angle of attack by disregarding the effects of the supersonic region at the leading edge, while essentially retaining the hodograph image for the case of the zero angle of attack. In the present paper the abovementioned complexities are avoided by enforcing a subsonic flow through the choice of a wedge with a round nose (figure 3c).

The mapping of the round nose of the wedge is as follows. The stagnation point

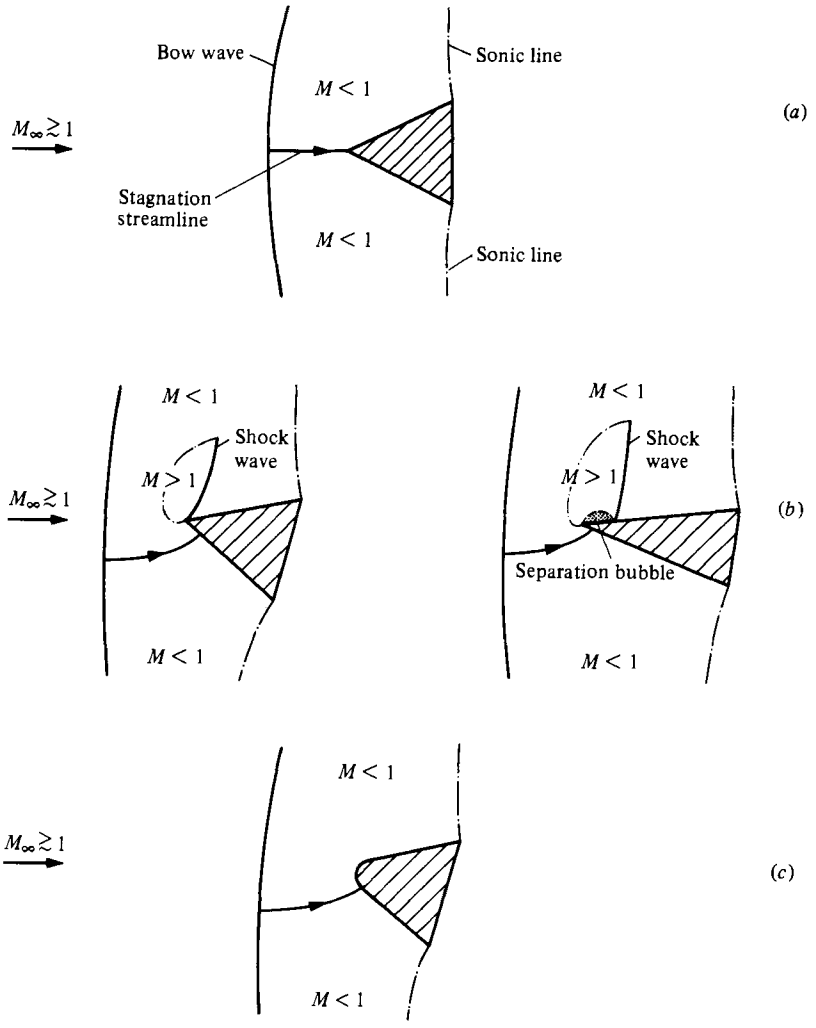

FIGURE 3. Flow field in the vicinity of the wedge with and without an angle of attack.

A appears again as the line $A'A''$ (figure 4), and the locations of the points A' and A'' in the hodograph plane are given through the directions of the flow β and $\beta-\pi$ respectively. The surface of the wedge is mapped on the curves $A'B_1B$ and $A''E_1E$ respectively, where the straight surfaces B_1B and E_1E of the wedge are now (owing to the angle of attack ϵ) situated at $\alpha-\epsilon$ and $-(\alpha+\epsilon)$ respectively. The mapping of the rounded nose in the hodograph plane is *a priori* unknown and has to be determined by the inverse method, i.e. an arbitrary curve of the rounded nose is chosen in the hodograph plane, the solution is subsequently computed and transformed to the physical plane. Usually the solution found is physically meaningless, because the computed wedge surface is found to intersect itself. Consequently some correction of the presumed curve in the hodograph plane has to be made and the computation scheme repeated until a smooth curve is finally obtained in the physical plane.

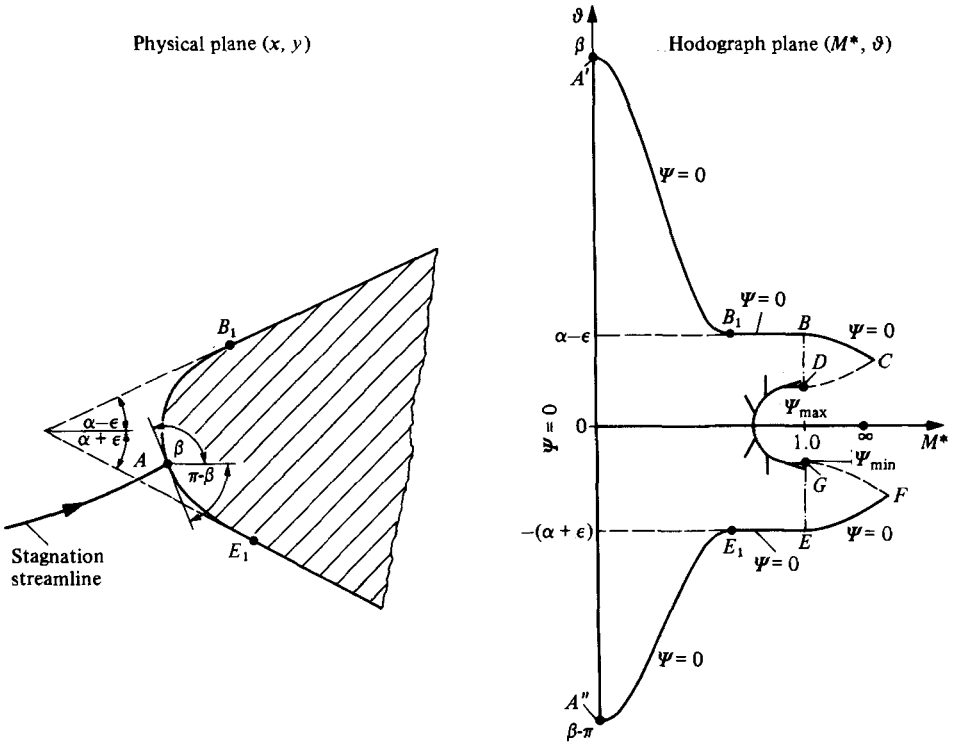

FIGURE 4. Mapping and formulation of the problem for the case of an angle of attack.

4. Numerical treatment of the problem

For an effective and accurate treatment of the problem with the finite-difference method a suitable coordinate system is indispensible. Diverse coordinate generators were used for the discretization of the elliptic field, whereas a net of characteristic curves was always used for the hyperbolic region. In figure 5 the solution $\Psi(M^*, \vartheta)$ is represented in the hodograph plane for a free-stream Mach number $M_\infty = 1.1$ past a wedge of half-angle 15°; the figure shows a rapid variation of Ψ near the intersection of the shock polar and the sonic line. This variation of the solution Ψ is much steeper and more pronounced for $M_\infty \gtrsim 1$ and gives an idea of the numerical difficulties encountered through the hodograph transformation.

The convenient and flexible technique of Thompson, Thames & Mastin (1977) for the numerical generation of boundary-fitted coordinates seemed very promising for the present problem. Computations with these coordinates, however, proved to be inaccurate, as will be demonstrated in §5. Aside from the mentioned inaccuracies near corners, this coordinate generator adversely affected the convergence of the relaxation technique for the elliptic region and the iteration scheme between the hyperbolic and elliptic regions. Very surprising was the fact that the method failed for $M_\infty \gtrsim 1, \alpha \ll 1$ and yielded absurd results. The determination of proper forcing functions also proved to be a tedious and very difficult task, which can be avoided by a modified method suggested by Middlecoff & Thomas (1979). In spite of this advantage, computations with these coordinates showed the same shortcomings mentioned previously.

No convergence could be achieved with a graded lattice in both directions similar to the one also unsuccessfully used by Vincenti & Wagoner (1952). The same

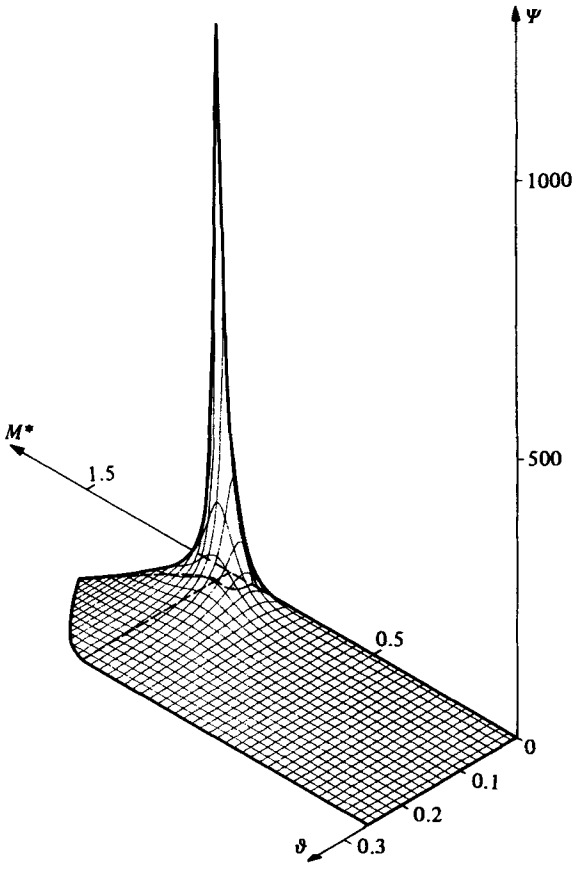

FIGURE 5. Perspective view of the stream function Ψ in the hodograph plane. $M_\infty = 1.1$, $\alpha = 15°$, $\epsilon = 0°$.

difficulties have been reported by van Raay (1978, private communication). Using a graded lattice in the M^* direction, convergence was achieved only for higher Mach numbers.

In contrast with the abovementioned systems, a square mesh proved to be favourable with regard to convergence and accuracy, and was therefore mainly used. Besides the treatment of irregular points (which, however, caused no difficulties) the great disadvantage of the Cartesian coordinates that were used lies in the necessity for a great number of grid points to obtain acceptable results. The discretizations of the elliptic and hyperbolic regions were done in a similar way to that described in Vincenti & Wagoner (1952) and Vincenti *et al.* (1956). For further details the reader is referred to Abboud (1982).

The system of finite-difference equations was solved by an iterative process between the elliptic and the hyperbolic regions. The peculiarity of the Chaplygin equation (3.1) is the change of its type in the domain under consideration. The equation is elliptic for $M^* < 1$ and hyperbolic for $M^* > 1$. For a mathematically appropriate treatment of both the elliptic and the hyperbolic regions, the value of Ψ on the sonic line BD is required (figure 2). These values of the stream function are, however, unknown *a priori*, and must be computed as part of the solution. This problem is solved by the following iterative scheme.

In the first stage of the computation the hyperbolic region is solved with the method

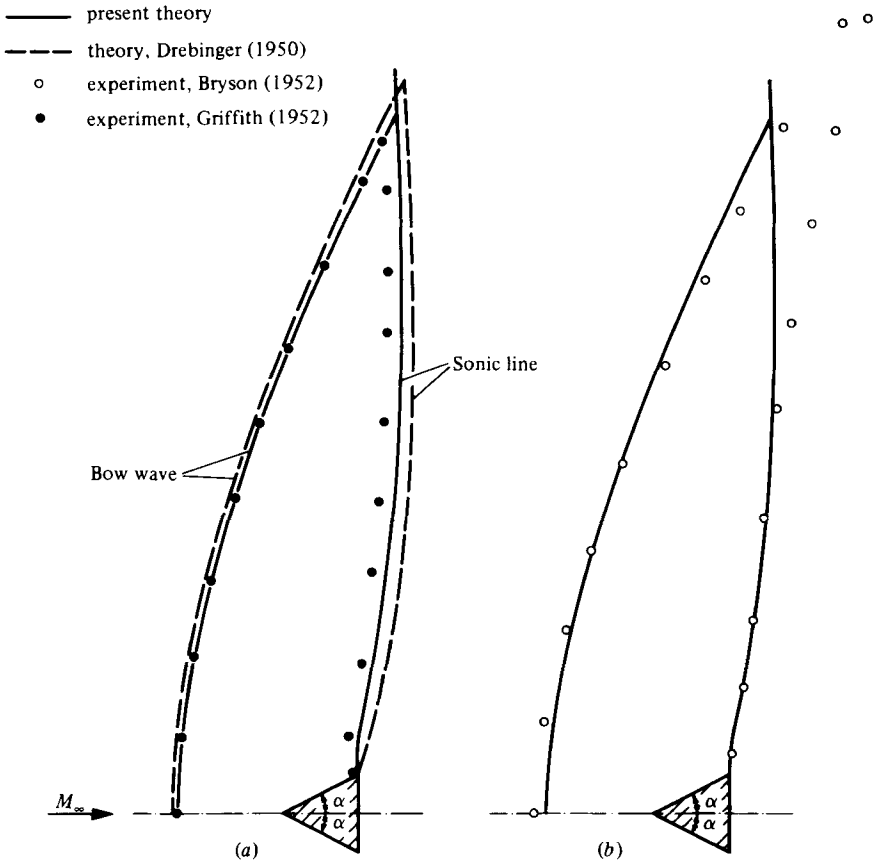

FIGURE 6. Comparison of the flow field with experiments of Griffith (1952) and Bryson (1952). $M_\infty = 1.44$, $\alpha = 26.6°$, $\epsilon = 0°$.

of characteristics by using guessed values of Ψ on the sonic line BD and the boundary condition $\Psi = 0$ on BC. Likewise the elliptic field is solved by a relaxation technique (SOR) using the pertinent boundary conditions (3.2) and the same guessed values of Ψ on the sonic line. In the second stage of the computation, the finite-difference version of (3.1) is solved for the sonic line, obtaining a new set of values for Ψ on that line, which are again used as new boundary conditions for both the elliptic and hyperbolic regions. The entire process is then repeated until a consistent solution is obtained for the whole domain.

5. Discussion of the results

After solving the boundary-value problem for Ψ using the iterative process described in §4 the solution must be transformed back to the physical plane. This is done by numerical integration of the relevant transformation formulas between the two planes. Details are omitted here, because a similar treatment can be found in Vincenti *et al.* (1956).

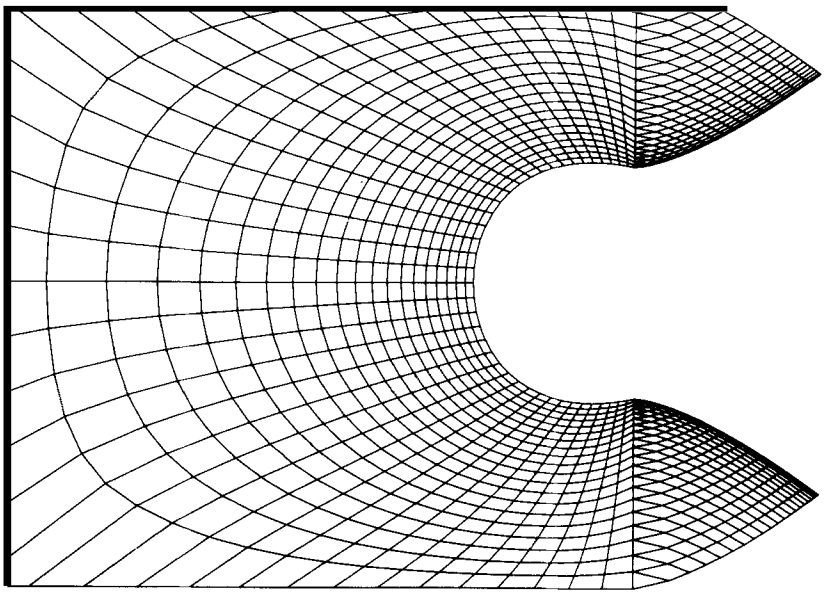

FIGURE 7. Boundary-fitted coordinates after Thompson *et al.* (1977). $M_\infty = 1.44$, $\alpha = 26.6°$, $\epsilon = 0°$.

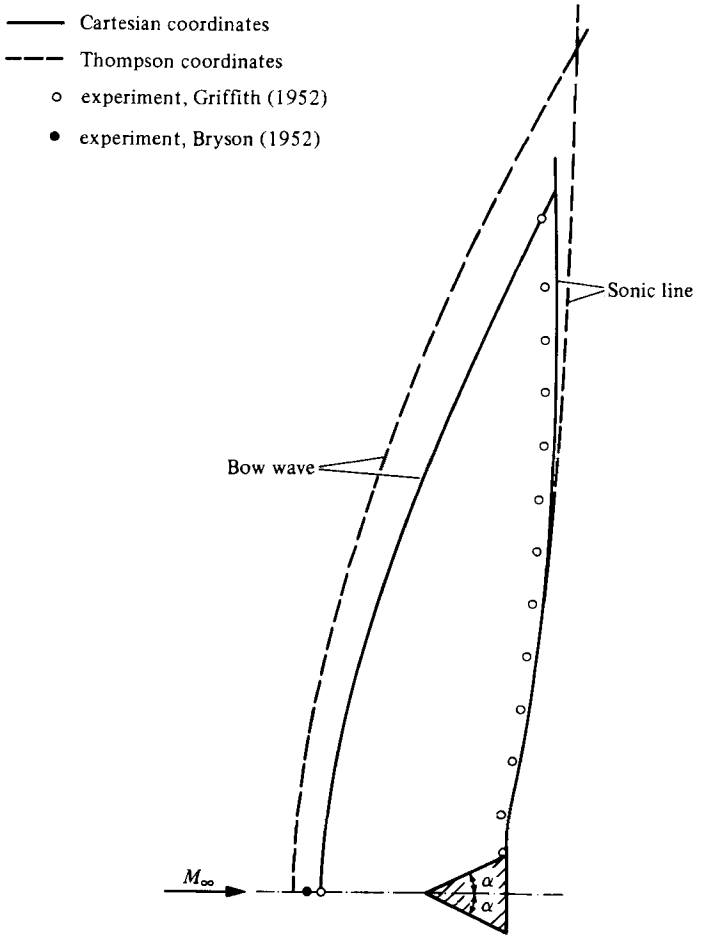

FIGURE 8. Flow field using Cartesian and numerical boundary-fitted coordinates. $M_\infty = 1.44$, $\alpha = 26.6°$, $\epsilon = 0°$.

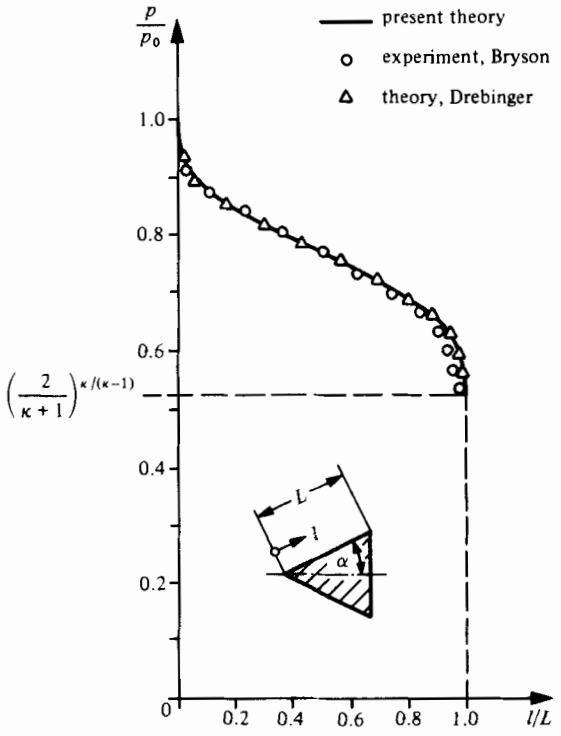

FIGURE 9. Pressure distribution on the wedge surface compared with the theory of Drebinger (1950) and experiments of Bryson (1952): $M_\infty = 1.44$, $\alpha = 26.6°$, $\epsilon = 0°$.

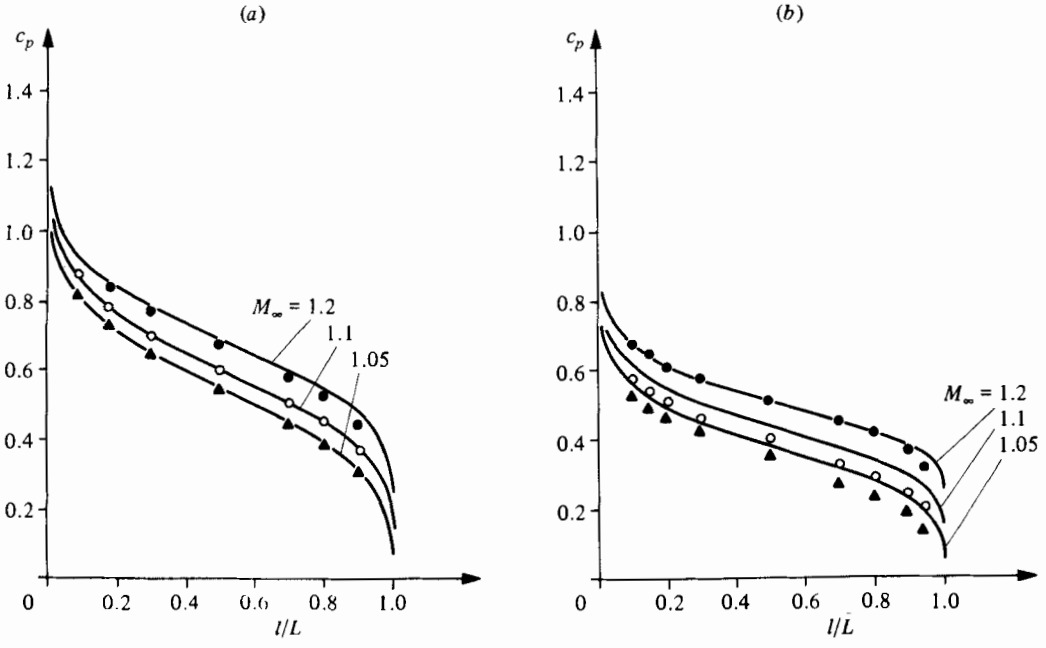

FIGURE 10. Pressure distribution on the wedge surface in comparison with experiments of Tanner (1978). (*a*) $\alpha = 15°$, $\epsilon = 0°$; (*b*) $\alpha = 7.5°$, $\epsilon = 0°$. Present theory: ——. Experiment: ●, $M_\infty = 1.2$; ○, 1.1; ▲, 1.05.

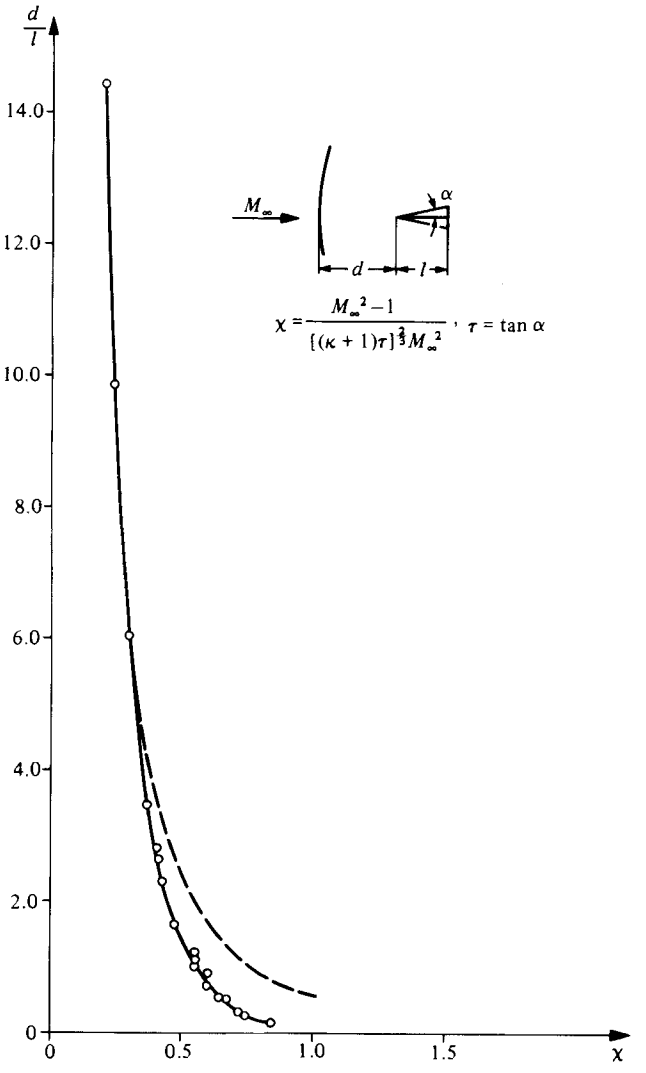

FIGURE 11. Shock stand-off distance d as a function of the transonic similarity parameter χ. ——, present theory for case $1.05 \leqslant M_\infty \leqslant 1.230$ and $0.05 \leqslant \tau \leqslant 0.176$; – – – theory (Zierep 1968), $d/l = \bar{a}^2/\chi^2$, $\bar{a} = 0.76$.

5.1. *Flow field, pressure and shock stand-off distance*

Figure 6(*a*) shows the shape of the bow wave and sonic line for the flow past a relatively thick wedge ($\tau = 0.5$) at a free-stream Mach number $M_\infty = 1.44$. The number of the grid points used in this computation was approximately 6000 for the elliptic and 600 for the hyperbolic region. The comparison with both the computation of Drebinger (1950), which was done in the physical plane and allows for an entropy gradient across the streamlines, and the experiments of Griffith (1952) in the shock tube shows good agreement. The deviation in the sonic line between theory and experiment can be explained through the development of the boundary layer on the wedge surface. It is interesting to note the differences (figure 6*b*) between the experimental results of Griffith (1952) and Bryson (1952). It can also be observed that the endpoints of the computed shock wave and sonic line do not meet at a common

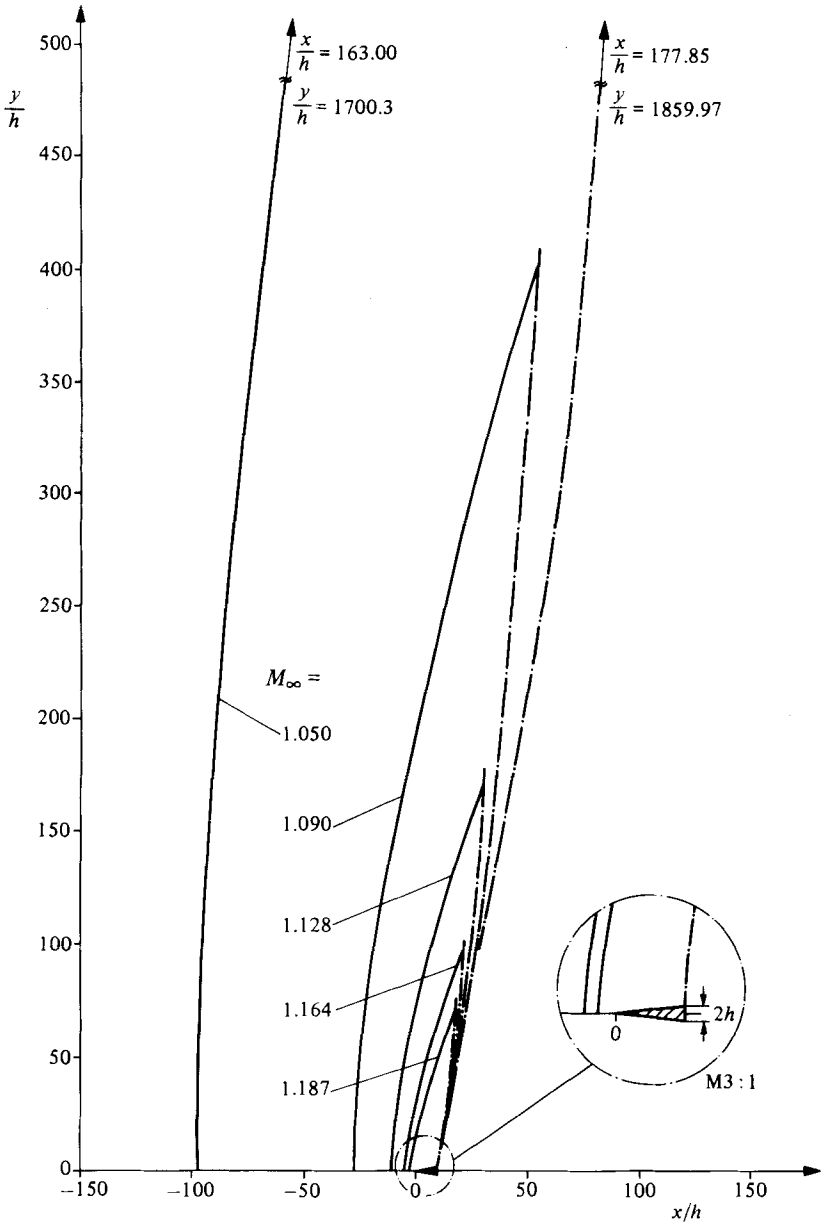

FIGURE 12. Influence of the free-stream Mach number M_∞ on the flow field. ——, bow wave; –·–·–, sonic line. $h \equiv$ half-thickness of wedge; $\alpha = 5.71°$, $\epsilon = 0°$.

point. This discrepancy is due to the high gradients of the stream function in the hodograph plane (figure 5) and the ultimate numerical inaccuracies made by building the necessary derivatives of Ψ for the transformation to the physical plane.

A comparison of the same flow field for Cartesian and numerically generated boundary-fitted coordinates (figure 7) after Thompson *et al.* (1977) is shown in figure 8. For orientation purposes the experimental shock stand-off distance of Griffith and Bryson as well as the sonic line of Griffith are drawn. The greater extension of the subsonic field for the numerical coordinates is due to small numerical inaccuracies

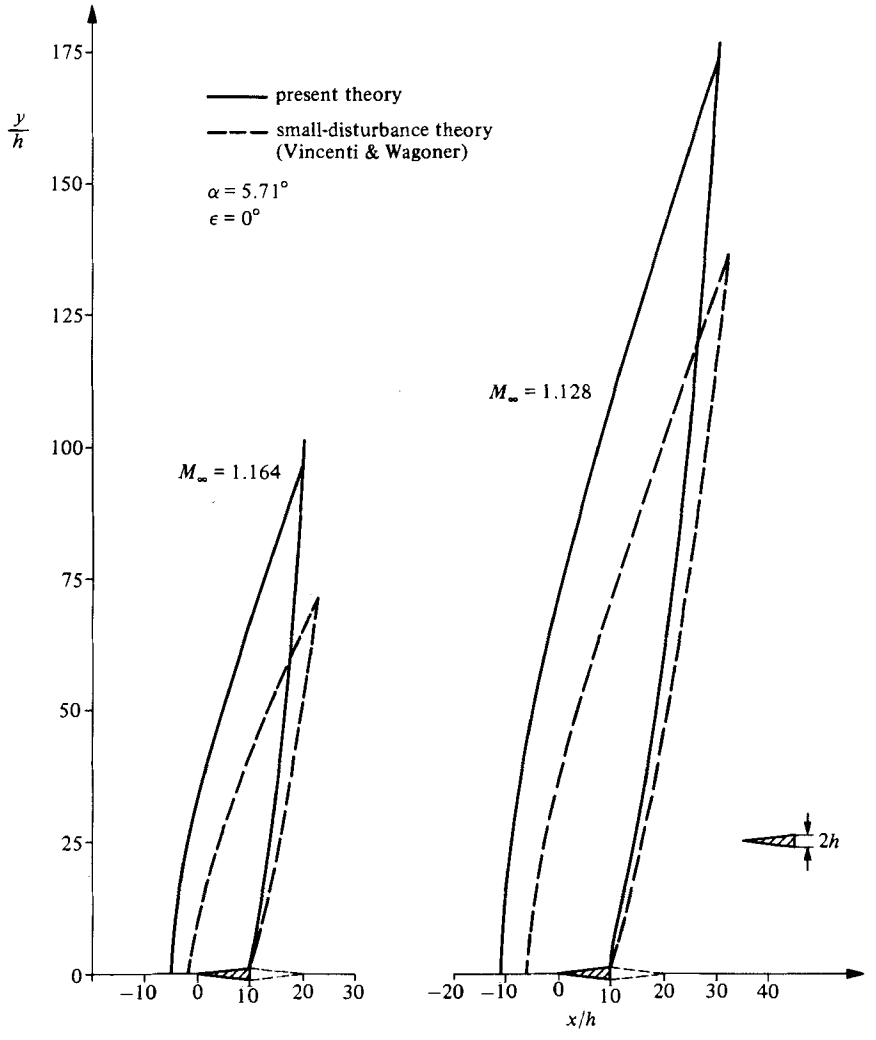

FIGURE 13. Comparison of the flow field with the small-disturbance theory after Vincenti & Wagoner (1982).

in the neighbourhood of the stagnation point A producing a smaller value for the half-thickness h of the wedge, which was used for making all distances dimensionless (see e.g. van Raay 1973). The ratio of pressure on the wedge surface to the stagnation pressure behind the shock is shown in figure 9.

Figure 10 shows a comparison of the computed pressure coefficient c_p on the wedge surface with experiments of Tanner (1978). The discrepancy between the two results for the thinner wedge at $M_\infty = 1.05$ and $M_\infty = 1.1$ is surprising since the agreement in all other cases is satisfactory.

In figure 11 the dimensionless shock stand-off distance d/l is plotted as a function of the transonic similarity parameter χ. The agreement with the theory of Zierep (1968) based on the frozen property of transonic flow and the asymptotic representation for the velocity after Müller & Matschat (1964) is very good for $\chi \leqslant 0.33$.

The influence of the free-stream Mach number M_∞ on the flow field past a wedge with the half-angle $\alpha = 5.71°$ ($\tau = 0.1$) is represented in figure 12. The extension of

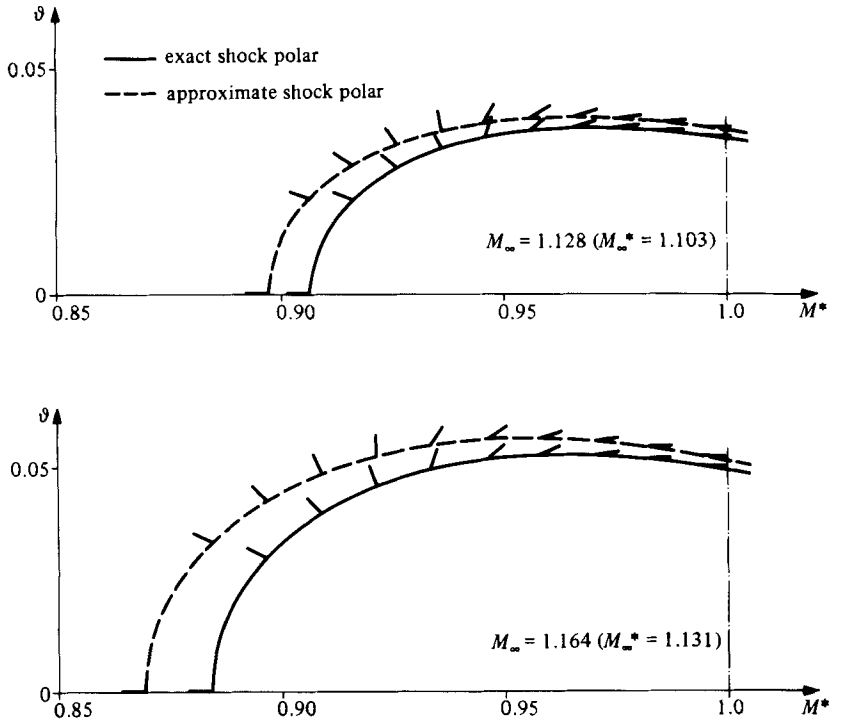

FIGURE 14. Exact and small-disturbance shock polar with streamlines.

the subsonic field in the vertical direction for $M_\infty = 1.05$ is very impressive. The endpoint of the bow wave at this free-stream Mach number for the flow past a wedge with the half-thickness $h = 1$ cm lies approximately 17 m above the profile!

5.2. *Comparison with the small-disturbance theory*

Of special interest is a quantitative comparison of the results with those of the small-disturbance theory. The assumption of this theory is that the velocity in the entire flow field differs only slightly from the critical speed of sound c^*. This leads to a mathematical simplification of the Chaplygin equation (3.1) to the Tricomi equation, which has the fundamental advantage of formulating a boundary condition for the stream function on the sonic line and allows a separate treatment of the elliptic and hyperbolic regions (see Vincenti & Wagoner 1952). The boundary condition (3.2*b*) for the slope of the streamlines on the shock polar is also simplified within the scope of this theory. A comparison of the flow field between the bow wave and the sonic line for the two theories is drawn in figure 13. It is apparent that the small-disturbance theory yields a smaller shock stand-off distance and a smaller extension of the subsonic region. The reason for these results becomes obvious when the shock polar with the slope of the streamlines is considered for the two cases (figure 14). The small-disturbance shock polar and the slope of the streamlines thereon correspond namely to an exact shock polar for a higher free-stream Mach number.

Besides this qualitative explanation, it is also possible to determine exactly the inclination of the shock wave at its intersection with the sonic line, which gives angles of $\Theta = 69.59°$ and $\Theta = 71.46°$ for $M_\infty = 1.164$ and $M_\infty = 1.128$ respectively. The numerical computation yields the angles $\Theta = 69.66°$ and $\Theta = 71.56°$ whereas the

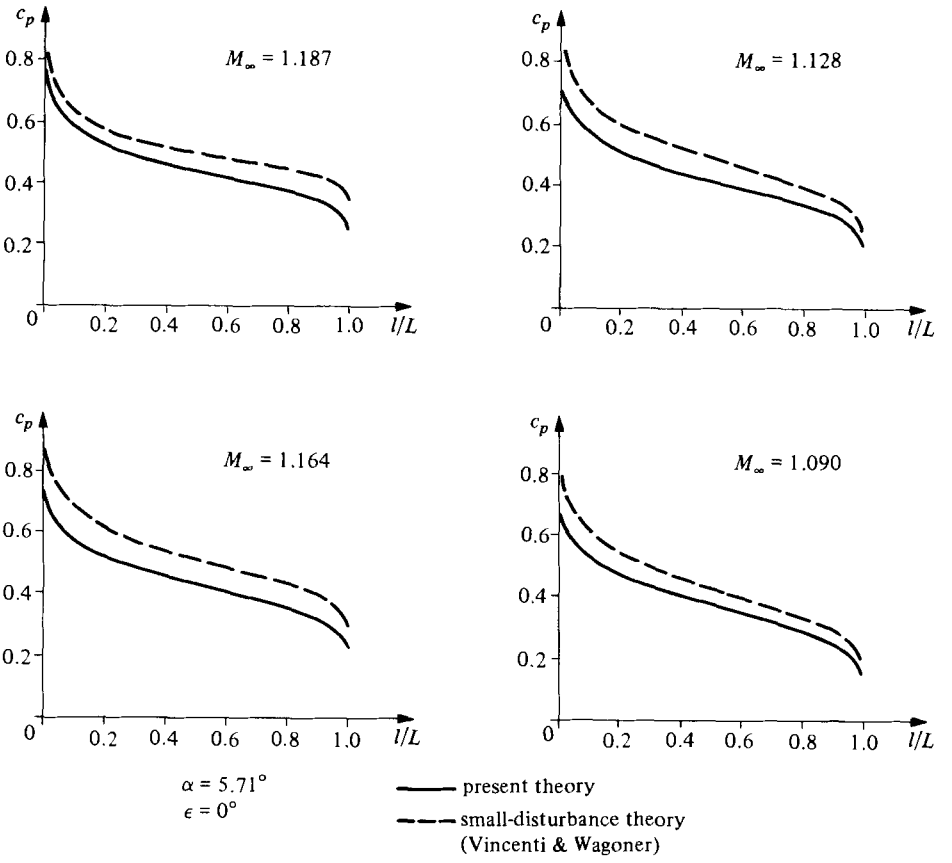

FIGURE 15. Comparison of pressure coefficient on the wedge surface with the small-disturbance theory after Vincenti & Wagoner (1952).

values depicted by the small-disturbance theory are $\Theta \approx 65.8°$ and $\Theta \approx 69.8°$ respectively.

The abovementioned remarks also find their counterpart in the pressure distribution on the wedge surface, which is illustrated in figure 15.

5.3. *Comparison with the flow at free-stream Mach number* 1

The limiting case of the flow past wedges at free-stream Mach number 1 has been treated both theoretically and experimentally by van Raay (1973). Figure 16 shows the distribution of the critical Mach number M^* along the stagnation streamline for the flow past several wedges at a free-stream Mach number $M_\infty = 1.2$. The forwards effect of the different profile thickness is clearly seen by comparing the case of flat plate ($\alpha = 90°$) and the thinnest wedge ($\alpha = 7.5°$). Closely related to the above is the velocity distribution on the wedge surface (figure 17). The very good agreement with the results of van Raay (1973), which were also calculated in the hodograph plane for the limiting case of $M_\infty = 1$, is very remarkable indeed.

5.4. *The rounded-off wedge with and without angle of attack*

In this section an example for the flow past rounded-off wedges with and without an angle of attack is treated using the inverse method. The computations are done with a relatively big mesh size, so that the shapes of the sonic line and the limiting

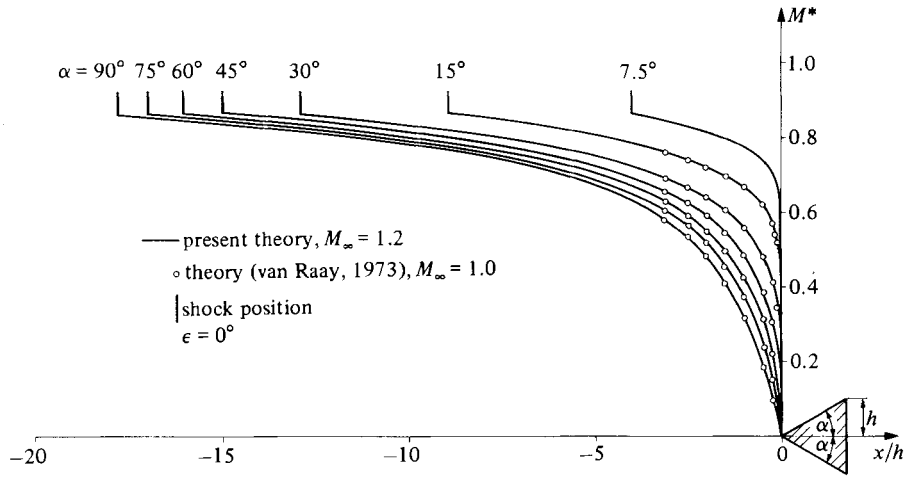

FIGURE 16. Distribution of the critical Mach number on the stagnation streamline for different wedges at $M_\infty = 1.2$, $7.5° \leqslant \alpha \leqslant 90°$, $\epsilon = 0°$.

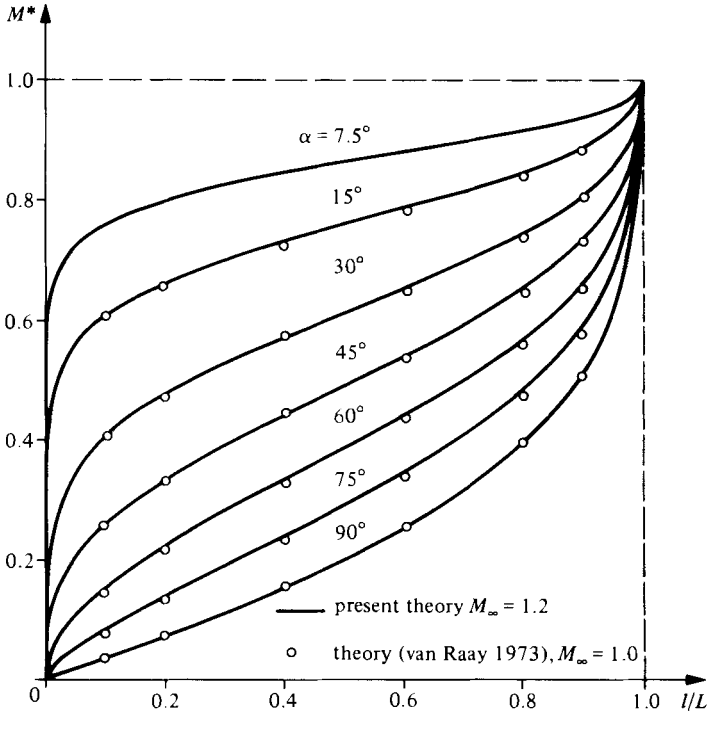

FIGURE 17. Distribution of the critical Mach number on the profile surface for different wedges at $M_\infty = 1.2$, $7.5° \leqslant \alpha \leqslant 90°$, $\epsilon = 0°$.

wave show inaccuracies in the vicinity of shock wave. However, the shock stand-off distance is accurate, as was demonstrated by test computations with different lattice intervals for the sharp wedge.

Figure 18 shows the image in the hodograph plane for the flow past three rounded-off wedges having the same half-angle $\alpha = 26.6°$ at a free-stream Mach number

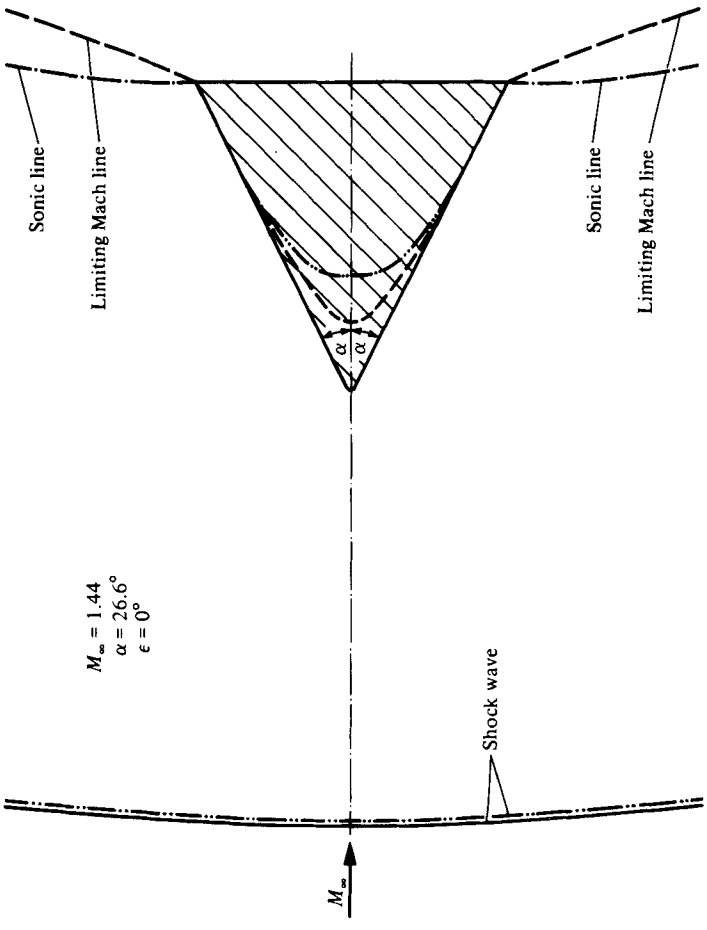

FIGURE 19. Flow past a wedge with three different rounded noses.

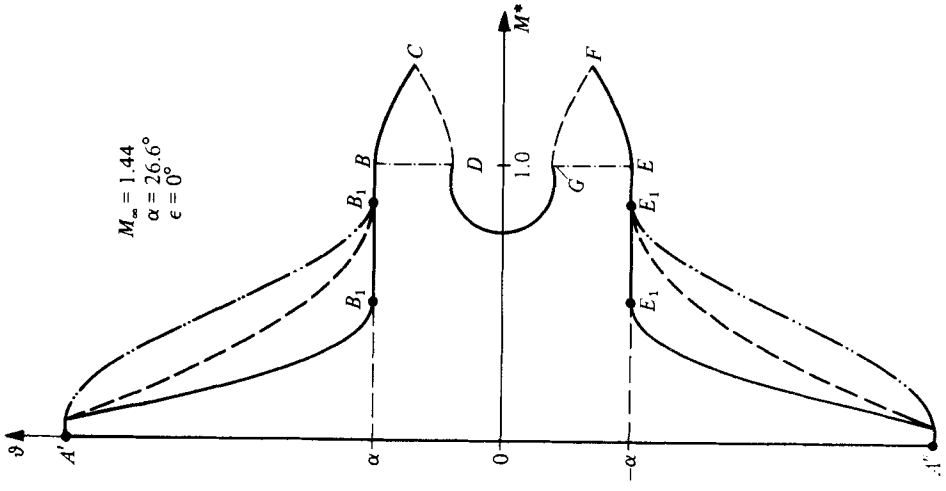

FIGURE 18. Hodograph image of a wedge with three different rounded noses.

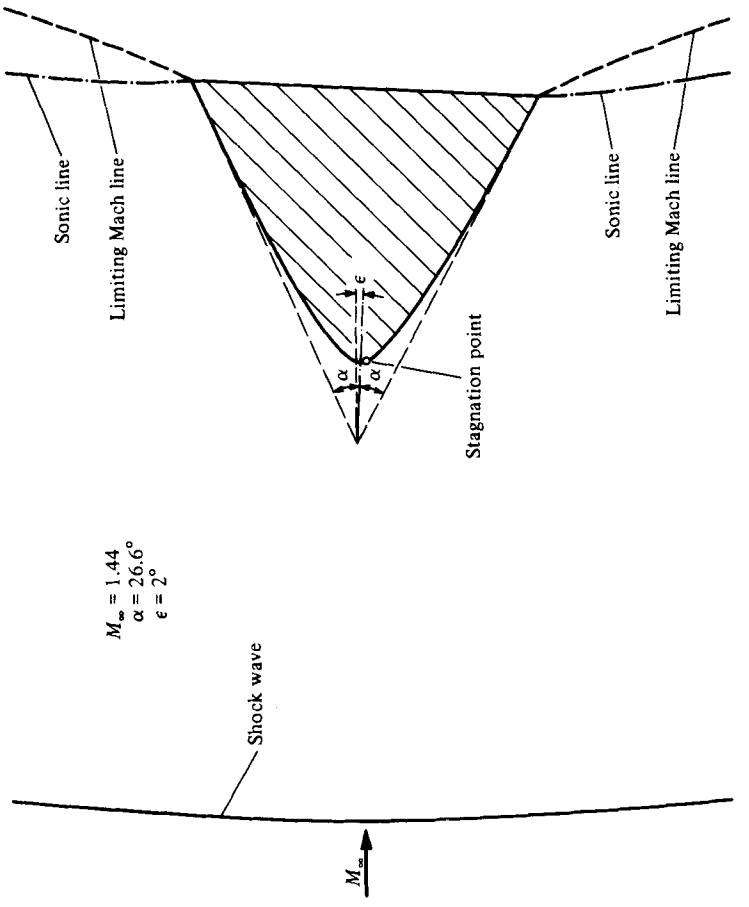

FIGURE 21. Flow field for the wedge with a rounded nose at an angle of attack.

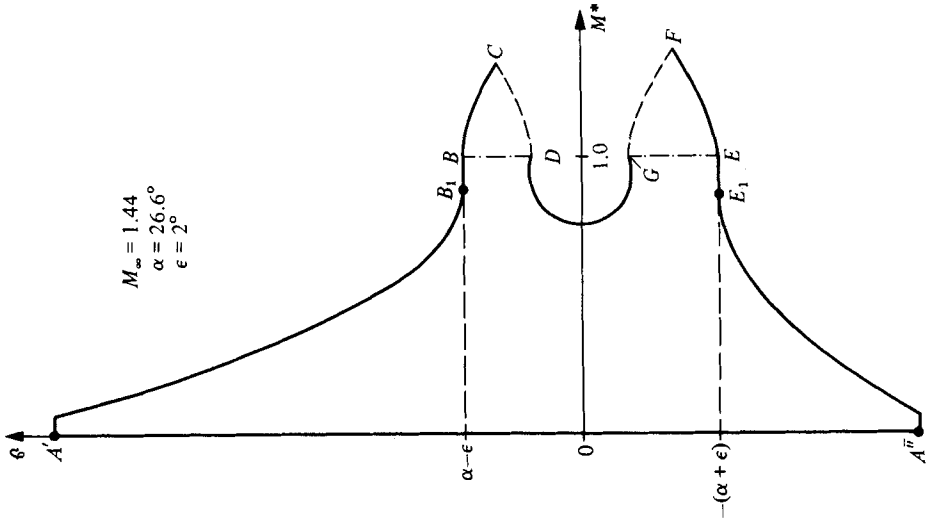

FIGURE 20. Hodograph image of a wedge with an angle of attack.

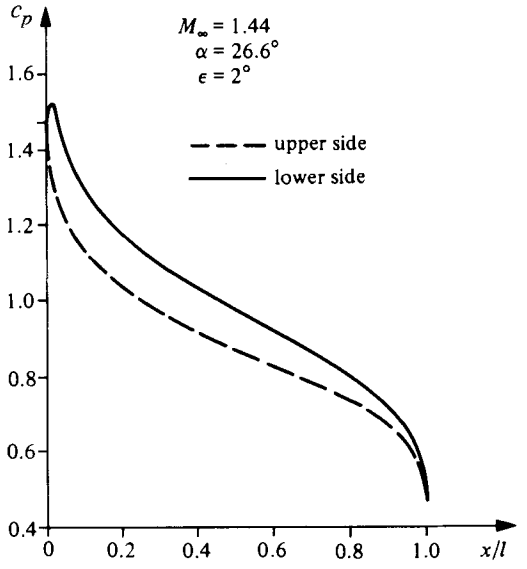

FIGURE 22. Pressure distribution for the wedge with a rounded nose at an angle of attack.

$M_\infty = 1.44$. The corresponding solution in the physical plane is sketched in figure 19. It is evident that the rounding of the nose enlarges the distance between the shock wave and the apex of the wedge, whereas the shock stand-off distance measured from the sonic line remains nearly unchanged.

As already mentioned in §3.4, the development of a local supersonic field at the leading edge for the case of an angle of attack can be avoided by rounding off the apex of the wedge. In addition to the previously described problem of finding the proper image of the rounded nose in the hodograph plane, a definite ratio of Ψ_{max} to Ψ_{min} must be iteratively determined, so that the two sides of the wedge will be of equal lengths. A choice of $\Psi_{min} = -\Psi_{max}$ (symmetrical case) yields different lengths for the upper and lower surface.

The hodograph image for the flow past a wedge with a rounded nose for the parameter combination $M_\infty = 1.44$, $\alpha = 26.6°$ and $\epsilon = 2°$ is sketched in figure 20. The solution on the physical plane is represented in figure 21. A comparison with the case of zero angle of attack (figure 19, middle contour) shows that the shock stand-off distance for this relatively thick profile ($\tau = 0.5$) remains unchanged. At this juncture it should be pointed out that the solution in the physical plane is very sensitive towards changes of the hodograph image. Small deviations from the right hodograph image lead to nonsensical contours in the physical plane.

The pressure coefficient for the upper and lower side of the wedge (figure 22) shows clearly the effect of the angle of attack ϵ.

6. Concluding remarks

The computation of the mixed subsonic–supersonic flow field past wedge profiles with detached shock waves using the hodograph method shows good agreement with other theories and experiments.

A comparison of the results of the small-disturbance theory (Tricomi equation) with the exact theory (Chaplygin equation) reveals that the former predicts both a smaller subsonic region as well as a higher pressure distribution on the surface of the profiles.

A very remarkable result is the very good agreement of the velocity distribution on the stagnation streamline, including the surface of the profile, for the free-stream Mach numbers $M_\infty = 1.2$ and $M_\infty = 1$ irrespective of the wedge thickness.

The great advantages of the hodograph method, namely the linearity of the differential equation, the known positions of the shock wave and limiting Mach wave, are offset by two difficulties. The first one is due to numerical complications caused through the very quick variation of the solution in the vicinity of the sonic line and shock polar. The second difficulty is the well-known fact that the problem past arbitrary rounded wedges is only susceptible to indirect treatment through the inverse method. Both difficulties proved to be formidable.

The author would like to thank his colleague Dr O. van Raay for the numerous and valuable discussions during the course of this work.

REFERENCES

ABBOUD, M. 1982 Die schallnahe Überschallumströmung von Keilen. Doctoral dissertation, Universität Karlsruhe.

BRYSON, A. E. 1952 An experimental investigation of transonic flow past two-dimensional wedge and circular-arc sections using a Mach–Zehnder interferometer. *NACA Rep.* 1094.

DREBINGER, J. W. 1950 Detached shock waves. Ph.D. thesis, Harvard University.

FERRARI, C. & TRICOMI, F. G. 1968 *Transonic Aerodynamics*. Academic.

FRANKL, F. 1947 On the problems of Chaplygin for mixed sub- and supersonic flows. *NACA TM* 1155.

GRAEFE, V. 1980 Berechnung des gemischten Unterschall-Überschall-Strömungsfeldes vor Keilen mit abgelöstem Verdichtungsstoß. Doctoral dissertation, Universität Clausthal.

GRIFFITH, W. 1952 Shock-tube studies of transonic flow over wedge profiles. *J. Aero. Sci.* **19**, 249–257.

GUDERLEY, K. G. 1947 Considerations on the structure of mixed subsonic–supersonic flow patterns. *Wright-Field Tech. Rep.* F-TR-2168-ND.

GUDERLEY, K. G. & YOSHIHARA, H. 1950 The flow over a wedge profile at Mach number 1. *J. Aero. Sci.* **17**, 723–735.

GUDERLEY, K. G. & YOSHIHARA, H. 1953 Two-dimensional unsymmetric flow patterns at Mach number 1. *J. Aero. Sci.* **20**, 757–768.

MIDDLECOFF, J. F. & THOMAS, P. D. 1979 Direct control of the grid point distribution in meshes generated by elliptic equations. In *A Collection of Technical Papers*, pp. 175–179. AIAA.

MÜLLER, E. A. & MATSCHAT, K. 1964 Ähnlichkeitslösungen der transsonischen Gleichung bei der Anströmmachzahl 1. In *Proc. Intl Congr. Appl. Mech.*, pp. 1061–1068.

SAUER, R. 1960 *Einführung in die theoretische Gasdynamik*. Springer.

TANNER, M. 1978 Druckverteilungsmessungen an Keilen bei Unterschall- und Transschallgeschwindigkeiten. *DVLR-FB* 78–22.

THOMPSON, J. F., THAMES, F. C. & MASTIN, C. W. 1977 Boundary-fitted curvilinear coordinate systems for solution of partial differential equations on fields containing any number of arbitrary two-dimensional bodies. *NASA* CR-2729.

VAN RAAY, O. 1973 Eine numerische Lösung der transsonischen Umströmung stumpfer Keilflanken. *Acta Mech.* **16**, 221–240.

VINCENTI, W. G. & WAGONER, C. B. 1952 Transonic flow past a wedge profile with detached bow wave. *NACA Rep.* 1095.

VINCENTI, W. G. & WAGONER, C. B. 1954 Theoretical study of the transonic lift of a double-wedge profile with detached bow wave. *NACA Rep.* 1180.

VINCENTI, W. G., WAGONER, C. B. & FISHER, N. H. 1956 Calculations of the flow over an inclined flat plate at free-stream Mach number 1. *NACA TN* 3723.

ZIEREP, J. 1968 Der Kopfwellenabstand bei einem spitzen, schlanken Körper in schallnaher Überschallanströmung. *Acta Mech.* **5**, 204–208.